

1 **Diagnostics of the ionospheric conductivity based on**
2 **spacecraft observations of the magnetospheric ULF**
3 **waves**

4 **E. E. Smotrova¹, P. N. Mager¹, O.S. Mikhailova¹, D. Yu. Klimushkin¹**

5 ¹Institute of Solar-Terrestrial Physics SB RAS, Irkutsk, Russia

6 **Key Points:**

- 7 • A method for estimating the ionospheric conductivity based on spacecraft obser-
8 vations of Alfvén waves in the magnetosphere is proposed
9 • The parallel structure of an Alfvén wave under various conditions of the ionospheric
10 conductivity is reconstructed
11 • The height-integrated Pedersen conductivity of the ionosphere were estimated for
12 the October 27, 2012 event

Corresponding author: E. E. Smotrova, katerina.smotrova@mail.iszf.irk.ru

Abstract

In 27 October 2012 the ULF wave in Pc4 range being Alfvén wave was observed with Van Allen Probe A. In the event the parallel Poynting flux of the wave was directed towards the Northern ionosphere. Assuming that this may be caused by the asymmetry of ionospheric conductivity between the Northern and Southern hemispheres, its effect on the standing structure of the Alfvén wave was investigated in this paper. For this purpose the analytical model with straight magnetic field lines was used. As a result the method for estimation of the Northern and Southern ionospheric conductivity was developed. It allows us to reconstruct the parallel structure of Alfvén waves under various conditions of the ionospheric conductivity. With the method developed, the ionospheric conductivity for the October 27, 2012 event was evaluated and compared with ionosphere model IRI-2016.

Plain Language Summary

The most commonly observed ULF waves in the magnetosphere are Alfvén waves standing along magnetic field line between magnetically conjugated points of the ionosphere located in opposite hemispheres. In this paper we considered how the north-south asymmetry of the ionospheric conductivity influences on standing Alfvén wave's parallel structure. The model predicts that the structure of the Alfvén waves may differ depending on the conductivity values of Northern and Southern ionospheres. Based on the model we developed the method to carry out a qualitative estimation of the ionospheric height-integrated Pedersen conductivity using parameters of Alfvén waves observed with spacecraft in the magnetosphere. As a result, for the 27 October 2012 event the parallel structure of the observed Alfvén wave was reconstructed and the ionospheric conductivity was estimated. We found a significant difference in the conductivity values of the Northern and Southern ionospheres. The mean is that the magnetically conjugated footprints of spacecraft trajectory, where the event observed, were located on different sides from the line that divides the day side and the night side of Earth (terminator line).

1 Introduction

Studies of the coupled system of ionosphere-magnetosphere is of crucial importance for the plasma processes in the near-Earth's space. An important part of this system is the ultra low frequency (ULF) waves, observed both in space and on the ground. The ULF waves are the field line oscillations with frequencies of the order or lower than the proton gyrofrequency. The most widespread classification categorizes these wave into regular pulsations Pc1–5 ranges (periods from 0.2 to 600 s) and irregular Pi1–2 pulsations (periods from 1 to 150 s) (Jacobs et al., 1964). These waves are interpreted in terms of magnetohydrodynamic (MHD) oscillations. Major part of the ULF waves are identified with the Alfvén waves standing along the field line between the magnetically conjugated points of ionosphere (Dungey, 1954; Radoski, 1967; Chen & Hasegawa, 1974; Southwood, 1974).

Standing Alfvén waves are often used for the diagnostics of the magnetospheric plasma (Troitskaya & Gul'elmi, 1967; Chi & Russell, 2005; Menk & Waters, 2013). Indeed, the Alfvén speed is inversely proportional to square root of the mass density, thus the observed wave's frequency allows one to reproduce plasma density distribution (Berube et al., 2006; Takahashi & Denton, 2007). A number of papers were devoted to calculation of the structure of the standing Alfvén waves with different distributions of density and other magnetospheric parameters (Cummings et al., 1969; Orr & Matthew, 1971; Allan & Knox, 1979a; Leonovich & Mazur, 1993; Ozeke & Mann, 2004; Pilipenko et al., 2005; Degeling et al., 2010; Petrashchuk et al., 2022).

61 However, there is yet another factor influencing wave's structure and frequency, the
 62 ionospheric conductivity. The studies of the influence of the conductivity on the stand-
 63 ing Alfvén waves began with works (Scholer, 1970; Inoue, 1973; Maltsev et al., 1974; Hughes,
 64 1974; Hughes & Southwood, 1976). Those papers considered ionosphere as a thin layer,
 65 which is justified for the long-period ULF waves (Pi2, Pc4–5). It was shown that the in-
 66 cident wave's magnetic field is reflected from the ionosphere due to the Pedersen con-
 67 ductivity, while the electric field reaches the ground due to the Hall conductivity. Fur-
 68 ther investigations of the ionosphere-magnetosphere interaction by means of the Alfvén
 69 waves were performed in (Alperovich & Fedorov, 1984; Glassmeier, 1984; Hameiri & Kivel-
 70 son, 1991; Leonovich & Mazur, 1991, 1996; Yoshikawa & Itonaga, 1996; Yoshikawa et al.,
 71 2002; Sciffer & Waters, 2002; Cheremnykh & Parnowski, 2006; Erkaev et al., 2006; Wa-
 72 ters et al., 2013).

73 Two limiting cases are worth mentioning. If the conductivity is high, then the wave's
 74 electric field equals zero on the ionosphere: $E_{\pm} = 0$, where the “+” and “-” signs refer
 75 to the conjugate ionospheres. In this case, the oscillating magnetic field line behave
 76 as if fixed in the points of intersection with the ionosphere. This oscillation is usually
 77 called the “rigid-end” mode (Cummings et al., 1969; Sinha & Rajaram, 1997).

78 In the opposite case, the conductivity is very small. In this case, the field aligned
 79 derivative of the wave's electric field equals zero on the ionosphere: $(\partial E/\partial l)_{\pm} = 0$, where
 80 l is a length along the field line. As a result the field line freely slides on the ionosphere.
 81 Such mode is called the “free-end mode” (Newton et al., 1978; Allan & Knox, 1979a).
 82 In both cases, between the conjugate ionospheres fit an integer half-waves, the Alfvén
 83 waves standing along the field line with no energy flux in this direction.

84 However, the situation is possible where the conductivities on the Northern and
 85 Southern magnetically conjugated points are drastically different. It can be caused by
 86 the asymmetry of Pedersen conductivity between the Northern and Southern hemispheres.
 87 This situation can occur in the polar ionosphere near the solstices, when one hemisphere
 88 is illuminated for a long time and the other is correspondingly in darkness (Glassmeier
 89 et al., 1999). In this case, a situation is possible where one end of the field line is fixed,
 90 and the other freely slides on the ionosphere. Then between the conjugate ionospheres
 91 fit an integer quarter-waves. For the first time, such possibility was mentioned in (Allan
 92 & Knox, 1979a). Results of further theoretical studies of the quarter-waves were reported
 93 in (Allan & Knox, 1979b; Allan, 1983; Bulusu et al., 2014, 2016). The observational ev-
 94 idences for the quarter-waves were presented in (Allan, 1983; Budnik et al., 1998; Bu-
 95 lusu et al., 2015; Obana et al., 2008, 2015).

96 The observational manifestations of the Alfvén waves at the asymmetric ionospheres
 97 are different from those in the symmetric case. Indeed, the frequency of the leading quarter-
 98 wave harmonic approximately two times lower than for the half-wave, there is field aligned
 99 energy flux. Thus, the Alfvén waves can be used for diagnostics of the ionosphere (Lee
 100 et al., 2004; Ozeke & Mann, 2004; Bulusu et al., 2015; Bulusu et al., 2016; Lysak et al.,
 101 2020).

102 Usually, ionospheric conductivities are determined in several ways. One method
 103 is based on the using of the models of the atmosphere, ionosphere and magnetic field with
 104 equations derived in (Maeda, 1977). For example, paper (Obana et al., 2015) used the
 105 atmosphere model MSISE-90, the ionosphere model IRI 95, and near-Earth geomagnetic
 106 field model IGRF 95. In another method the ground based instruments are used. The
 107 difficulty here appears in the necessity to use either data of combined observations from
 108 different instruments, for example, all sky cameras and riometers (Senior et al., 2008);
 109 either, special radar measurement programs and empirical models ought to be used (Ieda
 110 et al., 2014). Also, the low-orbital satellite data can be used, like SWARM mission. In
 111 the case of single satellite, calculation of the ionospheric conductivity demands using rather

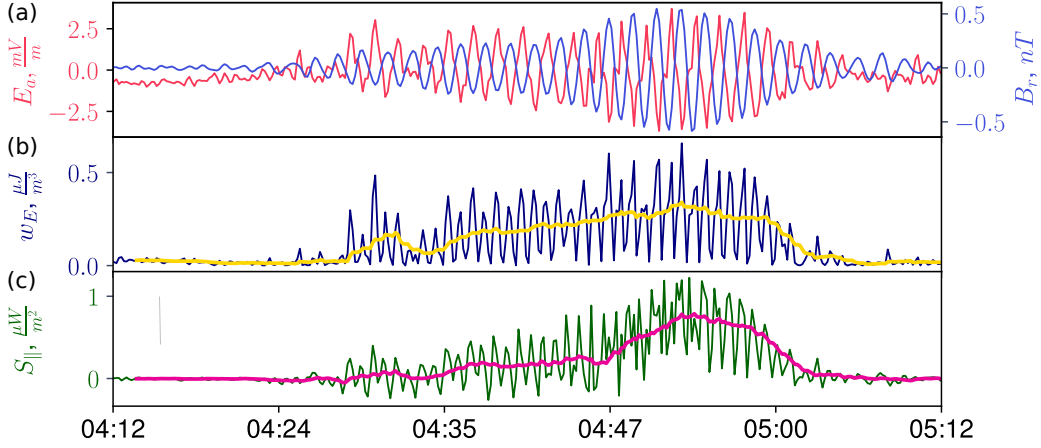


Figure 1. Peculiarities during the 27 October 2012 event: (a) the radial component of the wave’s magnetic field B_r (blue line) and the azimuthal component of the wave’s electric field E_a (red line); (b) the electric field energy density w_E (dark blue line) and \bar{w}_E (yellow line) averaged over the wave period $T = 100$ c (c) the same for parallel Poynting flux S_{\parallel} (green line) and \bar{S}_{\parallel} (red line).

112 complicated method which give results only along the satellite trajectory (Juusola et al.,
 113 2016).

114 2 27 October 2012 wave event

115 Let us consider the 27 October 2012 event, in which a poloidal Alfvén wave was
 116 observed with The Van Allen Probe A. The wave was registered in the morning part of
 117 the magnetosphere at a distance $6.2R_E$. During the event we observed the resonance
 118 generation of the ULF wave by the 38 keV electron flux. The electron flux was injected
 119 to the magnetosphere due to the substorm. The wave was the fundamental harmonic of
 120 the standing Alfvén wave with a frequency 10 mHz and azimuthal wave number $m \approx$
 121 $110 - 115$. The wave interacted with electrons via the drift resonance and was gener-
 122 ated through the gradient instability. The detailed study of the event is presented in (Mikhailova
 123 et al., 2022).

124 We revealed several peculiarities during the 27 October 2012 event studying, which
 125 were not mentioned in (Mikhailova et al., 2022). At the figure (Fig. 1) the wave field com-
 126 ponents, the electric field energy density w_E and the parallel Poynting flux S_{\parallel} , and their
 127 values averaged over the wave period $T = 100$ c are presented. One can see that phase
 128 shift between the radial component of the wave’s magnetic field B_r and the azimuthal
 129 component of the wave electric field E_a is about 180° , rather than 90° , as is usually ex-
 130 pected for standing waves. Moreover the Poynting flux was directed toward the North-
 131 ern ionosphere (Fig. 1b). We suggest that these observational peculiarities can be caused
 132 by the asymmetry of Pedersen conductivity between the Northern and Southern iono-
 133 spherics.

3 Principal equations

Let us consider the equation for an Alfvén wave. In the homogeneous background magnetic field and plasma it has a form:

$$\frac{\partial^2 E_j}{\partial l^2} + k_{\parallel}^2 E_j = 0, \quad (1)$$

where E_j is a component of the wave electric field (under index j is assumed r for the radial component and a for azimuthal one), $k_{\parallel} = \omega/v_A$ is the parallel component of wave vector, ω is the wave frequency, v_A is the Alfvén speed, l is a coordinate along the magnetic field line. The parallel component of electric field is not considered because it equals to zero in a MHD approximation. We assume the straight magnetic field lines.

The boundary condition for Alfvén waves on the ionosphere were determined in a lot of papers (Hughes, 1974; Hughes & Southwood, 1976; Newton et al., 1978; Leonovich & Mazur, 1991). It can be written in the form

$$E_j|_{l_{\pm}} = \mp i \frac{\epsilon^{\pm}}{k_{\parallel}} \frac{\partial E_j}{\partial l} \Big|_{l_{\pm}}, \quad (2)$$

where l_{\pm} is the coordinate of the Southern (l_-) and Northern (l_+) ionospheric boundaries, the dimensionless parameter ϵ^{\pm} is inversely proportional to the height-integrated Pedersen conductivity Σ_P^{\pm} ,

$$\epsilon^{\pm} = \frac{c^2}{4\pi\Sigma_P^{\pm}v_A}, \quad (3)$$

c is the speed of light. Eq. (2) assumes the field to enter to the ionosphere on the normal to it. For more general case, see (Leonovich & Mazur, 1991). The boundary condition (2) determines the damping decrement of the standing Alfvén wave under dissipation in the ionosphere. This one is caused by ionospheric Joule heating at the field line basement (Southwood & Hughes, 1983).

We use the coordinate $l_- = 0$ as a coordinate of the Southern ionosphere boundary and $l_+ = l_I$ as a coordinate of the Northern one. The length of the magnetic field line l_I can be obtained from the expression

$$l_I = LR_E \int_{-\theta_I}^{\theta_I} \sqrt{1 + 3 \sin^2 \theta} \cos \theta d\theta, \quad (4)$$

where L is a McIlwain parameter, $\pm\theta_I$ is the geomagnetic latitude of the Southern ($-$) and Northern ($+$) points of intersection of the magnetic field line with the ionosphere. The latitude can be found from the magnetic field line equation of the dipole magnetic field $r = LR_E \cos^2 \theta$, assuming $r = R_E + h_I$, where h_I is height of the upper boundary of the ionosphere (Chapman & Sugiura, 1956).

The dimensionless conductivity parameter ϵ^{\pm} (3) let us to take into account different values of Pedersen conductivity at the points of intersection. They are

1. High conductivity of the ionosphere at both the hemispheres: $\epsilon^{\pm} \ll 1$;
2. Low conductivity of the ionosphere at both the hemispheres: $\epsilon^{\pm} \gg 1$;
3. Asymmetric conductivity at the different hemispheres: $\epsilon^+ \gg 1, \epsilon^- \ll 1$.

It was assumed at all these cases that the ionospheric conductivities at the different hemispheres have the different absolute value.

The general solution of the wave equation (1) can be represented as

$$E_j = C_1 \exp(ik_{\parallel}l) + C_2 \exp(-ik_{\parallel}l). \quad (5)$$

170 Using boundary condition (2) we found the expression for the coefficients C_1 and C_2 , and
 171 equation for the parallel wave vector k_{\parallel} :

$$172 \quad (1 - \epsilon^-)(1 - \epsilon^+) \exp(ik_{\parallel}l_I) - (1 + \epsilon^-)(1 + \epsilon^+) \exp(-ik_{\parallel}l_I) = 0. \quad (6)$$

173 To solve (6) let us consider two limiting cases: (i) high conductivity, $\epsilon^{\pm} \ll 1$; (ii)
 174 low conductivity, $\epsilon^{\pm} \gg 1$. In both cases, the parallel wave vector can be represented
 175 in the form

$$176 \quad k_{\parallel} = k_0 + \delta k, \quad k_0 = \frac{\pi N}{l_I}, \quad (7)$$

177 where N is the harmonic wave number, and δk is a small addition caused by small value
 178 of ϵ^{\pm} in the first case and small value of $(\epsilon^{\pm})^{-1}$ in the second case. As result, we found
 179 the small value δk and the wave electric field, and, correspondingly, wave magnetic field

$$180 \quad B_a = -i \frac{c}{\omega} \frac{\partial E_r}{\partial l}, \quad B_r = i \frac{c}{\omega} \frac{\partial E_a}{\partial l} \quad (8)$$

181 the parallel Poynting flux averaged over the wave period

$$182 \quad \bar{S}_{\parallel} = \frac{c}{8\pi} (E_r B_a^* - E_a B_r^*). \quad (9)$$

183 In the case of high ionospheric conductivity, $\epsilon^{\pm} \ll 1$, the parallel structure of the
 184 wave's electromagnetic field is determined as

$$185 \quad E_{a,r} = \begin{pmatrix} E_{a0} \\ E_{r0} \end{pmatrix} \left[\sin k_0 l - i \left(\frac{\epsilon^- + \epsilon^+}{l_I} l - \epsilon^- \right) \cos k_0 l \right] \quad (10)$$

$$186 \quad B_{a,r} = \begin{pmatrix} -B_{a0} \\ B_{r0} \end{pmatrix} \left[\frac{\epsilon^- + \epsilon^+}{k_0 l_I} \cos k_0 l - \left(\frac{\epsilon^- + \epsilon^+}{l_I} l - \epsilon^- \right) \sin k_0 l + i \cos k_0 l \right] \quad (11)$$

187 where E_{a0} and E_{r0} are the amplitudes of the azimuthal and radial components of the
 188 wave electric field, and

$$189 \quad B_{a0} = E_{r0} \frac{k_0 c}{\omega}, \quad B_{r0} = E_{a0} \frac{k_0 c}{\omega} \quad (12)$$

190 are the amplitudes of the azimuthal and radial components of the wave magnetic field.

191 In the opposite low conductivity case, $\epsilon^{\pm} \gg 1$, the Alfvén wave's parallel struc-
 192 ture can be represented as

$$193 \quad E_{a,r} = \begin{pmatrix} E_{a0} \\ E_{r0} \end{pmatrix} \left[\cos k_0 l - i \left[\left(\frac{1}{\epsilon^-} + \frac{1}{\epsilon^+} \right) \frac{l}{l_I} - \frac{1}{\epsilon^-} \right] \sin k_0 l \right] \quad (13)$$

$$194 \quad B_{a,r} = \begin{pmatrix} -B_{a0} \\ B_{r0} \end{pmatrix} \left[\left(\frac{1}{\epsilon^-} + \frac{1}{\epsilon^+} \right) \frac{\sin k_0 l}{k_0 l_I} - \left[\left(\frac{1}{\epsilon^-} + \frac{1}{\epsilon^+} \right) \frac{l}{l_I} - \frac{1}{\epsilon^-} \right] \cos k_0 l + i \sin k_0 l \right] \quad (14)$$

195 For the case of the asymmetric ionosphere (low conductivity of the Northern iono-
 196 sphere, $\epsilon^+ \gg 1$, and high conductivity of the Southern ionosphere, $\epsilon^- \ll 1$, the par-
 197 allel wave vector is

$$198 \quad k_{\parallel} = \frac{1}{2} k_0 + \delta k \quad (15)$$

199 the parallel structure is represented as

$$200 \quad E_{a,r} = \begin{pmatrix} E_{a0} \\ E_{r0} \end{pmatrix} \left[\sin \frac{k_0 l}{2} - i \left[\left(\epsilon^- + \frac{1}{\epsilon^+} \right) \frac{l}{l_I} - \epsilon^- \right] \cos \frac{k_0 l}{2} \right] \quad (16)$$

$$201 \quad B_{a,r} = \frac{1}{2} \begin{pmatrix} -B_{a0} \\ B_{r0} \end{pmatrix} \left[2 \left(\epsilon^- + \frac{1}{\epsilon^+} \right) \frac{\cos \frac{k_0 l}{2}}{k_0 l_N} - \left[\left(\epsilon^- + \frac{1}{\epsilon^+} \right) \frac{l}{l_N} - \epsilon^- \right] \sin \frac{k_0 l}{2} + i \cos \frac{k_0 l}{2} \right] \quad (17)$$

202 Let us consider properties of the wave's parallel structure on the equator, where
 203 $l = l_I/2$. Expressions for the azimuthal component of the wave's electric field E_a , the

204 radial component of the magnetic field and the parallel Poynting flux S_{\parallel} are presented
 205 in Table 1, where $\Delta\phi$ is the phase shift between B_r and E_a components, and

$$206 \quad S_0 = \frac{c^2 k_0}{16\pi\omega} (E_{a0}^2 + E_{r0}^2). \quad (18)$$

207 It is worth to note that only the highest order terms are written.

Table 1. Expressions for the azimuthal component of the wave's electric field E_a , the radial component of the magnetic field and the parallel Poynting flux on the geomagnetic equator for the fundamental harmonic ($N = 1$)

Case	$E_a \left(\frac{l_I}{2}\right)$	$B_r \left(\frac{l_I}{2}\right)$	$\bar{S}_{\parallel} \left(\frac{l_I}{2}\right)$	$\Delta\phi$
$\epsilon^{\pm} \ll 1$	E_{a0}	$-\frac{B_{r0}}{2}(\epsilon^+ - \epsilon^-)$	$S_0(\epsilon^+ - \epsilon^-)$	$\sim 180^\circ, 0^\circ$
$\epsilon^{\pm} \gg 1$	$-i\frac{E_{a0}}{2} \left(\frac{1}{\epsilon^+} - \frac{1}{\epsilon^-}\right)$	iB_{r0}	$S_0 \left(\frac{1}{\epsilon^+} - \frac{1}{\epsilon^-}\right)$	$\sim 180^\circ, 0^\circ$
$\epsilon^+ \gg 1, \epsilon^- \ll 1$	$\frac{E_{a0}}{2\sqrt{2}}$	$i\frac{B_{r0}}{2\sqrt{2}}$	$S_0 \left[\frac{1}{2} \left(\frac{1}{\epsilon^+} - \epsilon^- \right) - \frac{1}{k_0 l_I} \left(\frac{1}{\epsilon^+} + \epsilon^- \right) \right]$	$\sim 90^\circ$

208

209 The following properties of the standing Alfvén wave on the geomagnetic equator
 210 are apparent from Table 1:

- 211 1. The phase shift between the electric E_a (E_r) and magnetic B_r (B_a) fields for the
 212 symmetric conditions is close to 180° or 0° , and for asymmetric conditions to 90° ;
- 213 2. Since conductivities $\Sigma_P^{\pm} \propto 1/\epsilon^{\pm}$, then for the symmetric conditions the absolute
 214 value and direction of the parallel Poynting flux S_{\parallel} is determined by the differ-
 215 ence of the ionospheric conductivities ($\epsilon^{\pm} \gg 1$ case) or their reverse values ($\epsilon^{\pm} \ll$
 216 1 case).
- 217 3. For the asymmetric conditions, the absolute value and direction of the parallel Poynt-
 218 ing flux is determined by the combination of the conductivity of one ionosphere
 219 and the conductivity reverse value of the other.

220 The correctness of the results is indicated by the coincidence of the phase shift under
 221 symmetric and asymmetric conditions at the boundaries of the ionosphere with early the-
 222 oretical work (Newton et al., 1978; Southwood & Kivelson, 2001).

223 4 Ionospheric conductivity estimation model

224 Expressions received for standing Alfvén wave allow to estimate ionospheric con-
 225 ductivity based on spacecraft data processing of observing magnetospheric Alfvén waves.
 226 Inputs include wave parameters such as its period or frequency and wave electric and
 227 magnetic field and spacecraft coordinates. Since $v_A = \omega/k_{\parallel}$ and $k_{\parallel} \approx k_0 \equiv \pi N/l_I$ for
 228 $\epsilon^{\pm} \ll 1$ and $\epsilon^{\pm} \gg 1$ symmetric cases, then as follows from eq. (3)

$$229 \quad \Sigma_P^{\pm} = \frac{c^2 k_0}{4\pi\omega\epsilon^{\pm}} = \frac{Nc^2}{4l_I\omega\epsilon^{\pm}} \quad (19)$$

230 where the length of magnetic field line l_I can be defined from (4).

231 With obtained model, the universal method of ionospheric conductivity estimation
 232 was developed. It is required to determine ratio between conductivities. For this point,
 233 the maximum value of the parallel Poynting flux averaged over the wave period \bar{S}_{\parallel} is used

234 (Fig. 1c). Also, the period-averaged energy density of the wave electric or magnetic field

$$235 \quad \bar{w}_E = \frac{1}{16\pi}(E_r E_r^* + E_a E_a^*), \quad \bar{w}_B = \frac{1}{16\pi}(B_r B_r^* + B_a B_a^*). \quad (20)$$

236 corresponding to this time is used. For example, as follows from Table 1 for the funda-
237 mental harmonic ($N = 1$) at the magnetic equator for $\epsilon^\pm \ll 1$ case we have

$$238 \quad \bar{w}_E = \frac{1}{16\pi}(E_{a0}^2 + E_{r0}^2). \quad (21)$$

239 and

$$240 \quad (\epsilon^+ - \epsilon^-) = \frac{\omega}{c^2 k_0} \frac{\bar{S}_\parallel}{\bar{w}_E}. \quad (22)$$

241 For $\epsilon^\pm \gg 1$ case we have

$$242 \quad \bar{w}_B = \frac{1}{16\pi}(B_{a0}^2 + B_{r0}^2) = \frac{c^2 k_0^2}{16\pi\omega^2}(E_{a0}^2 + E_{r0}^2). \quad (23)$$

243 and

$$244 \quad \left(\frac{1}{\epsilon^+} - \frac{1}{\epsilon^-} \right) = \frac{k_0}{\omega} \frac{\bar{S}_\parallel}{\bar{w}_B}. \quad (24)$$

245 If the height-integrated Pedersen conductivity of one ionosphere is known (for ex-
246 ample, Southern Σ_P^-), then using the observed values of the period-averaged parallel Poynt-
247 ing flux and energy density the conductivity of the other ionosphere (Northern Σ_P^+) can
248 be calculated with eq. (19) and eq. (22) or eq. (24) depending on the case under consid-
249 eration

250 The principle of operation is simple and requires only the availability of the data
251 from magnetospheric observation of Alfvén wave. Moreover, data from one spacecraft
252 is enough for the method to work. Note using method has disadvantage at this stage of
253 development. The fixed height-integrated Pedersen conductivity of one hemisphere is set
254 manually. This can be done using reference theoretical conductivity values or using other
255 empirical models or direct measurements. Thus, the characteristic height-integrated Ped-
256 ersen conductivity is of order of 10^8 km/s (~ 10 mho) for the daytime ionosphere and
257 10^7 km/s (~ 1 mho) for the nighttime ionosphere (Leonovich & Mazur, 1993; South-
258 wood & Hughes, 1983).

259 Let's obtain criterion for distinguishing cases of high and low ionospheric conduc-
260 tivity ("fixed-end" or "free-end" mode of Alfvén wave). Providing the wave is observed
261 near the geomagnetic equator, the expressions from Table. 1 are valid. For high conduc-
262 tive ionosphere, the difference between the dimensionless values of hemispheres conduc-
263 tivity according to Table. 1 is defined as:

$$264 \quad (\epsilon^+ - \epsilon^-) = -\frac{2\omega}{k_0 c} \frac{B_r}{E_a} \quad (25)$$

265 Since the ionosphere is high conductive medium $\epsilon^\pm \ll 1$, the relation between the
266 magnetic and electric field of the observed ULF wave is as follows:

$$267 \quad \left| \frac{2\omega}{k_0 c} \frac{B_r}{E_a} \right| \ll 1 \quad (26)$$

268 For the low ionospheric conductivity $\epsilon^\pm \gg 1$, the inverse dimensionless values of
269 hemispheres conductivity according to Table. 1 is written as:

$$270 \quad \left(\frac{1}{\epsilon^+} - \frac{1}{\epsilon^-} \right)^{-1} = -\frac{\omega}{2k_0 c} \frac{B_r}{E_a} \quad (27)$$

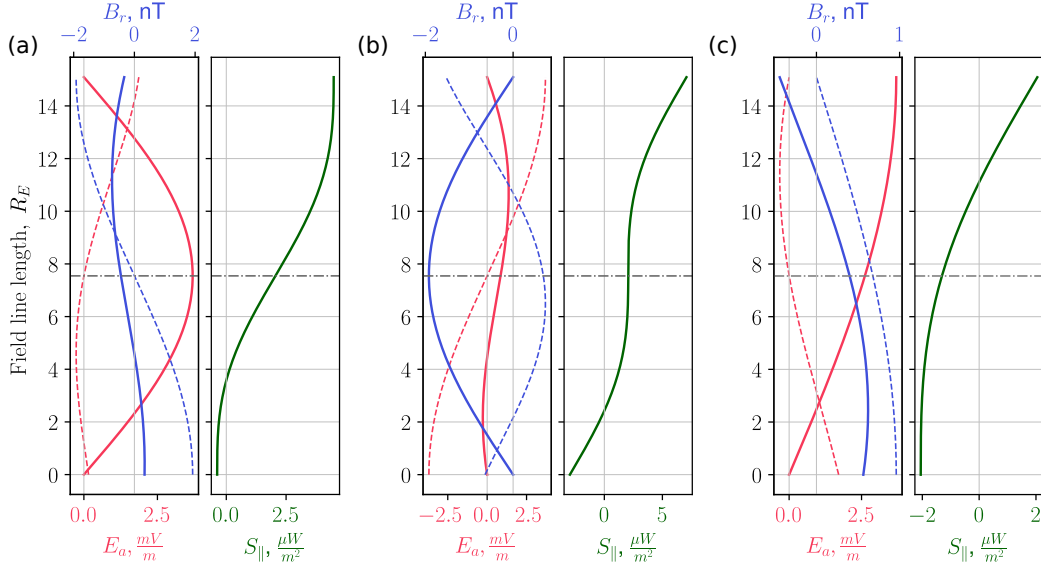


Figure 2. Parallel structure of the Alfvén wave and field aligned Poynting vector component calculated using the ionospheric conductivity estimation model for for the following cases: (a) $\epsilon^{\pm} \ll 1$, (b) $\epsilon^{\pm} \gg 1$, (c) $\epsilon^{+} \gg 1$, $\epsilon^{-} \ll 1$. The solid lines are the real part of calculated values, the dashed lines are the imaginary ones

271 Then using that fact that the ionosphere is low-conducting $\epsilon^{\pm} \gg 1$, we obtain next
 272 result for relation between magnetic and electric fields of the observed wave:

$$273 \left| \frac{\omega}{2k_0 c} \frac{B_r}{E_a} \right| \gg 1 \quad (28)$$

274 Criteria (26) and (28) means that the proposed parameter ϵ^{\pm} should be greater than
 275 unity in the case of low conductivity. Otherwise, there is a case of high ionospheric con-
 276 ductivity. The case when proposed criteria equal to unity is not considered due to the
 277 fact that the decay decrement will have a value of the order of the wave frequency. It
 278 means the wave attenuates very quickly and cannot exist.

279 5 Estimation ionospheric conductivity during the 27 October 2012 event

280 The event of 27 October 2012 was observed near geomagnetic equator. Thus, the
 281 model proposed in section 4 is applicable for estimation of ionospheric conductivity. Fig. 2
 282 shows an example of how, based on spacecraft data, it is possible to restore the stand-
 283 ing structure of the observed wave for different ionosphere conductivity conditions.

284 Phase shift between radial magnetic field and azimuthal electric field is about 180°
 285 for symmetric conditions on ionosphere (Fig.2a,b). Furthermore the case of asymmet-
 286 ric ionospheric conductivity represented on Fig.2c is not suitable because of the pecu-
 287 liarities of the observed wave.

288 The criteria (26) and (28) were checked for distinguishing symmetric conductiv-
 289 ity conditions on the ionosphere. The criterion (26) is met during the observed wave event.
 290 In this case one can conclude that ionospheric conductivity was high for both the hemi-
 291 spheres and the almost "fixed-end" mode of the wave was established. Then standing
 292 structure of the wave according to the simulation results had the forms as shown in the

293 Fig. 2a. Besides, we known that the observed wave was in the drift resonance with en-
 294 energetic electrons, and if ionospheric conductivity were low, then the azimuthal electric
 295 field of the wave would be asymmetrical and the drift resonance would not be observed.

296 According to the observational data and equations in Table 1 the difference between
 297 dimensionless conductivity parameters for both hemisphere $\epsilon^+ - \epsilon^-$ is equal to 0.476. It
 298 is assumed that the difference in the conductivity values may be caused by the fact that
 299 the footprints of the spacecraft trajectory, where the event observed, were located on dif-
 300 ferent sides from the terminator line. For verification, the Tsyganenko model T96 (Tsyganenko,
 301 1996) was used to calculate the spacecraft footprints. The terminator line was computed
 302 using the Cartopy library of the Python (Met Office, 2010 - 2015). The results are shown
 303 in Fig. 3 for the time 04:53 UT when the maximum value of parallel Poynting flux \overline{S}_{\parallel}
 304 was registered (Fig. 1a). At that time the spacecraft was located at the magnetic field
 305 line corresponding to the magnetic shell $L \approx 6.2R_E$. Fig. 3 shows that the northern
 306 footprint of spacecraft trajectory is located on the night-side ionosphere, and the south-
 307 ern one is on the day-side ionosphere.

308 As mentioned in section 4 in order to estimate height-integrated Pedersen conduc-
 309 tivity the fixed conductivity for one hemisphere is required to set up. In our research,
 310 height-integrated Pedersen conductivity in the Southern hemisphere (Σ_P^-) is given by the
 311 ionosphere model IRI-2016 (Bilitza et al., 2017). The values of height-integrated Ped-
 312 ersen conductivity is represented in Table 2 based on IRI-2016 model and our method.
 313 The order of value of the obtained height-integrated conductivities is consistent with the
 314 theoretical estimates from the papers (Southwood & Hughes, 1983; Leonovich & Mazur,
 315 1993) and observational results in (Obana et al., 2008; Ieda et al., 2014; Obana et al.,
 316 2015). Dimensionless conductivity parameter for the Northern hemisphere according to
 317 the IRI-2016 model is greater than one. Therefore, the observed wave must be the quarter-
 318 wave, what means the phase shift between electric and magnetic field of the wave should
 be around 90° . But according to spacecraft data, this is not observed (Fig. 1a).

Table 2. Height-integrated Pedersen conductivity for the Northern and Southern footprints of
 the magnetic field line on the 27 October 2012 according to the suggested method at 04:53 UT
 and the ionosphere model IRI-2016 at 05:00 UT. The last are taken at an altitude of 1000 km
 above sea

	IRI-2016	Our method
$\Sigma^-, \text{ mho (km/s)}$	9.610 (8.65×10^6)	
ϵ^-	0.043	
$\Sigma^+, \text{ mho (km/s)}$	0.190 (1.71×10^6)	0.795 (7.16×10^6)
ϵ^+	2.172	0.519

319
 320 There are two factors which can explain difference in the values of height-integrated
 321 Pedersen conductivity for Northern hemisphere Σ_P^+ . As shown in Fig. 3 the footprints
 322 of magnetic field line is located in polar region. In (Bjoland et al., 2016) with compared
 323 IRI-2016 model and EISCAT Svalbard radar, it was shown that at the high-latitudes re-
 324 gions model IRI-2016 can underestimate electron density. Another study (Lyakhov et
 325 al., 2019) also showed that in transit time (04-08 MLT, from nighttime to daytime), only
 326 25% of calculations based on the IRI-2016 model are within the instrumental accuracy
 327 of DE-2 satellite measurements ($0 \pm 15\%$). The model IRI-2016 may incorrectly take into

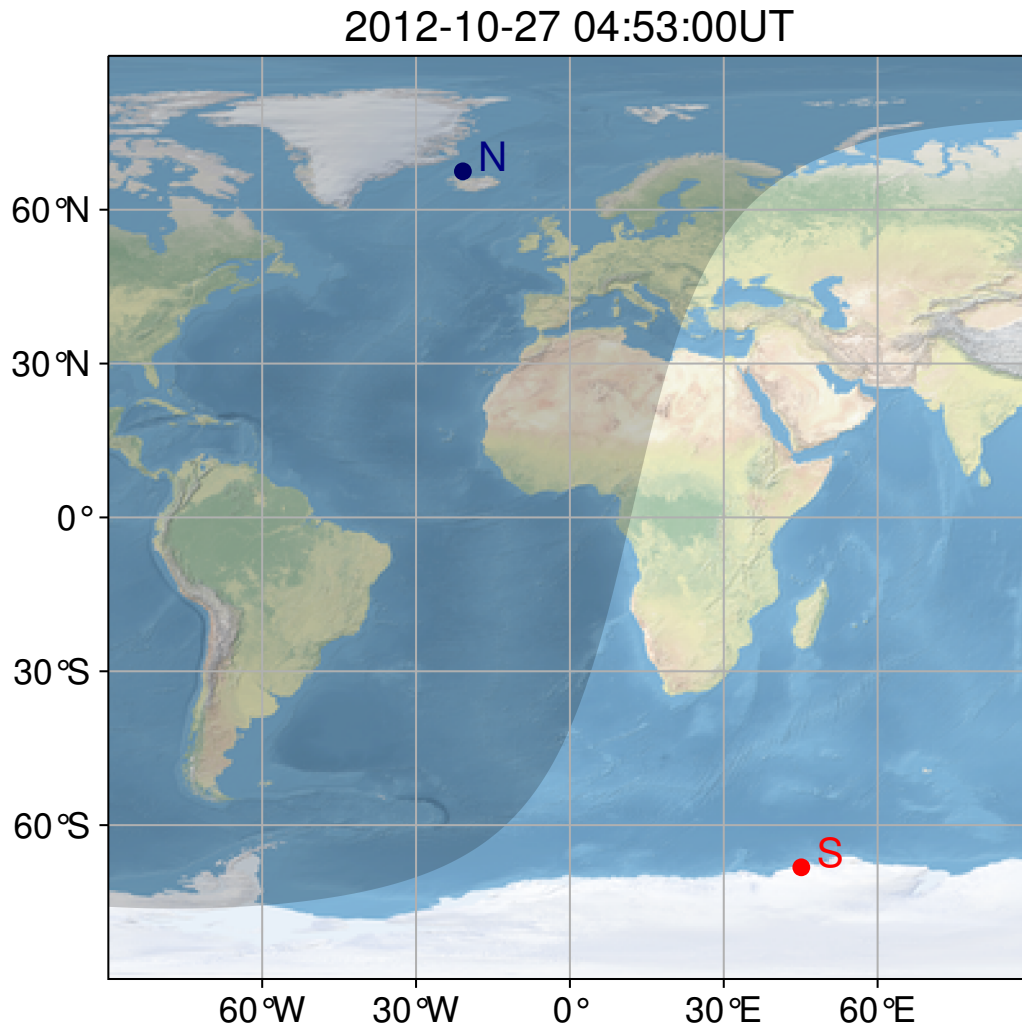


Figure 3. Terminator line and Northern (N) and Southern (S) footprints of the magnetic field line calculated using Tsyganenko model T96 (Tsyganenko, 1996) for the altitude 1000 km above the sea. The terminator and footprints were evaluated from data of event 27 October 2012 at 04:53 UT

328 account the conditions of the external ionosphere and twilight at all altitudes. Also, it
 329 can not properly consider the impact of ionization processes in night side ionosphere.

330 On the other hand, our proposed method is limited. The use of assumptions that
 331 the field enter to the ionosphere on the normal to it, straight magnetic field lines and
 332 the requirement of the wave be observed near the geomagnetic equator, influence esti-
 333 mation the relationship between the conductivities. However, the method shows the pos-
 334 sibility to use spacecraft data to estimate ionospheric conductivity and their influence
 335 on structure of standing Alfvén. The method can be improved by using the dipole model
 336 of the magnetic field.

337 6 Conclusion

338 The effect of different conductivity of the magnetically conjugated parts of the iono-
 339 sphere on the structure of standing Alfvén waves using an analytical model with straight
 340 magnetic field lines is considered in this paper. Based on the model, a method was de-
 341 veloped that allows to estimate the height-integrated Pedersen conductivity at magnet-
 342 ically conjugated points of the ionosphere with spacecraft observations of magnetospheric
 343 Alfvén waves. A criterion distinguishing the "fixed-end" and "free-end" of the half-wave
 344 mode of the standing Alfvén wave was also obtained from the model. Due to the pro-
 345 posed method, the observational features of the October 27, 2012 event were explained
 346 by the difference in conductivity values at the Northern and Southern ionosphere. Pro-
 347 ceeding to the criteria, a half-wave mode of the Alfvén wave with almost "fixed-end" at
 348 magnetically conjugated points of the ionosphere was proved to be observed for this event.
 349 With given Pedersen conductivity for the Southern ionosphere from IRI-2016 model, the
 350 conductivity for the Northern ionosphere was estimated. It is shown that the difference
 351 in the conductivity values are caused by the fact that footprints of spacecraft trajectory,
 352 where the event observed, were located on different sides from the terminator line.

353 Data Availability Statement

354 The Van Allen Probes data used in this paper are available at the CDAWeb site
 355 (<https://cdaweb.gsfc.nasa.gov/pub/data/rbsp/rbspa/>). The height-integrated Ped-
 356 ersen conductivity data are available at World Data Center for Geomagnetism, Kyoto
 357 (<https://wdc.kugi.kyoto-u.ac.jp/ionocond/sigcal/index.html>).

358 Acknowledgments

359 The work was financially supported by the Grant of the Russian Science Foundation (project
 360 No. 22-77-10032). We acknowledge the NASA Van Allen Probes and Craig Kletzing for
 361 use of EMFISIS data, John Wygant for use of EFW data.

362 References

- 363 Bjoland, L., Belyey, V., Løvhaug, U., & La Hoz, C. (2016). An evaluation of Inter-
 364 national Reference Ionosphere electron density in the polar cap and cusp using
 365 EISCAT Svalbard radar measurements. *Annales Geophysicae*, *34*, 751-758.
 366 doi: 10.5194/angeo-34-751-2016
- 367 Allan, W. (1983). Quarter-wave ulf pulsations. *Planetary and Space Science*, *31*(3),
 368 323-330. doi: 10.1016/0032-0633(83)90083-1
- 369 Allan, W., & Knox, F. B. (1979a). A dipole field model for axisymmetric Alfvén
 370 waves with finite ionosphere conductivities. *Planetary and Space Science*,
 371 *27*(1), 79-85. doi: 10.1016/0032-0633(79)90149-1
- 372 Allan, W., & Knox, F. B. (1979b). The effect of finite ionosphere conductivities on
 373 axisymmetric toroidal Alfvén wave resonances. *Planetary and Space Science*,

- 374 27(7), 939-950. doi: 10.1016/0032-0633(79)90024-2
- 375 Alperovich, L. S., & Fedorov, E. N. (1984). Effect of the ionosphere on the propaga-
376 tion of MHD wave beams. *Radiofizika*, 27(10), 1238-1247.
- 377 Berube, D., Moldwin, M. B., & Ahn, M. (2006). Computing magnetospheric mass
378 density from field line resonances in a realistic magnetic field geometry. *Jour-
379 nal of Geophysical Research: Space Physics*, 111(A8). doi: [https://doi.org/10.
380 .1029/2005JA011450](https://doi.org/10.1029/2005JA011450)
- 381 Bilitza, D., Altadill, D., Truhlik, V., Shubin, V., Galkin, I., Reinisch, B., & Huang,
382 X. (2017). International Reference Ionosphere 2016: From ionospheric cli-
383 mate to real-time weather predictions. *Space Weather*, 15, 418-429. doi:
384 10.1002/2016SW001593
- 385 Budnik, F., Stellmacher, M., Glassmeier, K.-H., & Buchert, S. C. (1998). Iono-
386 spheric conductance distribution and mhd wave structure: observation and
387 model. *Annales Geophysicae*, 16(2), 140-147. doi: 10.1007/s00585-998-0140-8
- 388 Bulusu, J., Sinha, A. K., & Vichare, G. (2014). Toroidal quarter waves in the
389 Earth's magnetosphere: theoretical studies. *Astrophys. Space Sci.*, 353, 395-
390 404. doi: 10.1007/s10509-014-2052-2
- 391 Bulusu, J., Sinha, A. K., & Vichare, G. (2015). An analytic model of toroidal
392 half-wave oscillations: Implication on plasma density estimates. *Journal of
393 Geophysical Research: Space Physics*, 120(6), 4164-4180. (2014JA020797) doi:
394 10.1002/2014JA020797
- 395 Bulusu, J., Sinha, A. K., & Vichare, G. (2015). Toroidal quarter waves in the
396 Earth's magnetosphere: observational perspective. *Astrophys. Space Sci.*,
397 357(1), 13. doi: 10.1007/s10509-015-2306-7
- 398 Bulusu, J., Sinha, A. K., & Vichare, G. (2016). Role of finite ionospheric conductiv-
399 ity on toroidal field line oscillations in the Earth's magnetosphere – Analytic
400 solutions. *Journal of Geophysical Research (Space Physics)*, 121(6), 5404-5421.
401 doi: 10.1002/2015JA022019
- 402 Chapman, S., & Sugiura, M. (1956). Arc-lengths along the lines of force of a mag-
403 netic dipole. *Journal of Geophysical Research*, 61(3), 485-488. doi: 10.1029/
404 jz061i003p00485
- 405 Chen, L., & Hasegawa, A. (1974). A theory of long period magnetic pulsation.
406 1: Steady state excitation of a field line resonance. *Journal of Geophysical Re-
407 search*, 79, 1024-1032. doi: 10.1029/JA079i007p01024
- 408 Cheremnykh, O. K., & Parnowski, A. S. (2006). Influence of ionospheric conduc-
409 tivity on the ballooning modes in the inner magnetosphere of the Earth. *Ad-
410 vances in Space Research*, 37(3), 599-603. doi: 10.1016/j.asr.2005.01.073
- 411 Chi, P. J., & Russell, C. T. (2005). Travel-time magnetoseismology: Magneto-
412 spheric sounding by timing the tremors in space. *Geophysical Research Letters*,
413 32(18). doi: <https://doi.org/10.1029/2005GL023441>
- 414 Cummings, W. D., O'Sullivan, R. J., & P. J., C., Jr. (1969). Standing Alfvén waves
415 in the magnetosphere. *Journal of Geophysical Research*, 74, 778. doi: 10.1029/
416 JA074i003p00778
- 417 Degeling, A. W., Rankin, R., Kabin, K., Rae, I. J., & Fenrich, F. R. (2010). Mod-
418 eling ULF waves in a compressed dipole magnetic field. *Journal of Geophysical
419 Research: Space Physics*, 115(A10), A10212. doi: 10.1029/2010JA015410
- 420 Dungey, J. W. (1954). Electrodynamics of the outer atmospheres. In *Ionospheric
421 science report, no 69* (p. 1-52). Ions. Res. Lab., Pennsylvania State Univ.
- 422 Erkaev, N. V., Shaidurov, V. A., Semenov, V. S., Biernat, H. K., & Heidorn, D.
423 (2006). Dissipation of Alfvén wave pulses propagating along dipole magnetic
424 tubes with reflections at the ionosphere. *Advances in Space Research*, 37(3),
425 576-580. doi: 10.1016/j.asr.2005.09.002
- 426 Glassmeier, K. H. (1984). On the influence of ionospheres with non-uniform conduc-
427 tivity distribution on hydromagnetic waves. *Journal of Geophysics Zeitschrift
428 Geophysik*, 54(2), 125-137.

- 429 Glassmeier, K.-H., Buchert, S., Motschmann, U., Korth, A., & Pedersen, A. (1999).
 430 Concerning the generation of geomagnetic giant pulsations by drift-bounce
 431 resonance ring current instabilities. *Annales Geophysicae*, *17*, 338–350. doi:
 432 10.1007/s00585-999-0338-4
- 433 Hameiri, E., & Kivelson, M. G. (1991). Magnetospheric waves and the atmosphere-
 434 ionosphere layer. *Journal of Geophysical Research*, *96*(A12), 21125–21134. doi:
 435 10.1029/91JA02129
- 436 Hughes, W. J. (1974). The effect of the atmosphere and ionosphere on long pe-
 437 riod magnetospheric micropulsations. *Planetary and Space Science*, *22*(8),
 438 1157–1172. doi: 10.1016/0032-0633(74)90001-4
- 439 Hughes, W. J., & Southwood, D. J. (1976). The screening of micropulsation signals
 440 by the atmosphere and ionosphere. *Journal of Geophysical Research*, *81*, 3234-
 441 3240. doi: 10.1029/JA081i019p03234
- 442 Ieda, A., Oyama, S., Vanhamäki, H., Fujii, R., Nakamizo, A., Amm, O., ... Nishi-
 443 tani, N. (2014). Approximate forms of daytime ionospheric conductance.
 444 *Journal of Geophysical Research: Space Physics*, *119*(12), 10,397–10,415. doi:
 445 https://doi.org/10.1002/2014JA020665
- 446 Inoue, Y. (1973). Wave polarizations of geomagnetic pulsations observed in high lat-
 447 itudes on the earth's surface. *Journal of Geophysical Research*, *78*(16), 2959-
 448 2976. doi: 10.1029/JA078i016p02959
- 449 Jacobs, J. A., Kato, Y., Matsushita, S., & Troitskaya, V. A. (1964). Classification of
 450 geomagnetic micropulsations. *Journal of Geophysical Research*, *69*(1), 180–181.
 451 doi: https://doi.org/10.1029/JZ069i001p00180
- 452 Juusola, L., Archer, W. E., Kauristie, K., Burchill, J. K., Vanhamäki, H., & Aikio,
 453 A. T. (2016). Ionospheric conductances and currents of a morning sector
 454 auroral arc from swarm-a electric and magnetic field measurements. *Geophys-
 455 ical Research Letters*, *43*(22), 11,519–11,527. doi: https://doi.org/10.1002/
 456 2016GL070248
- 457 Lee, D. H., Kim, K. H., Denton, R. E., & Takahashi, K. (2004). Effects of iono-
 458 spheric damping on MHD wave mode structure. *Earth, Planets and Space*, *56*,
 459 e33–e36. doi: 10.1186/BF03352541
- 460 Leonovich, A. S., & Mazur, V. A. (1991). An electromagnetic field, induced in
 461 the ionosphere and atmosphere and on the earth's surface by low-frequency
 462 Alfvén oscillations of the magnetosphere: General theory. *Planetary and Space
 463 Science*, *39*(4), 529–546. doi: 10.1016/0032-0633(91)90048-F
- 464 Leonovich, A. S., & Mazur, V. A. (1993). A theory of transverse small-scale stand-
 465 ing Alfvén waves in an axially symmetric magnetosphere. *Planetary and Space
 466 Science*, *41*, 697–717. doi: 10.1016/0032-0633(93)90055-7
- 467 Leonovich, A. S., & Mazur, V. A. (1996). Penetration to the Earth's surface of
 468 standing Alfvén waves excited by external currents in the ionosphere. *Annales
 469 Geophysicae*, *14*, 545–556. doi: 10.1007/s00585-996-0545-1
- 470 Lyakhov, A., Kozlov, S., & Bekker, S. (2019). Assessment of the Accuracy of
 471 Calculations Using the International Reference Ionosphere Model IRI-2016:
 472 I. Electron Densities. *Geomagnetism and Aeronomy*, *59*(1), 45–52. doi:
 473 10.1134/S0016793219010110
- 474 Lysak, R. L., Song, Y., Waters, C. L., Sciffer, M. D., & Obana, Y. (2020). Numerical
 475 investigations of interhemispheric asymmetry due to ionospheric conductance.
 476 *Journal of Geophysical Research: Space Physics*, *125*(7), e2020JA027866. doi:
 477 https://doi.org/10.1029/2020JA027866
- 478 Maeda, K. (1977). Conductivity and drifts in the ionosphere. *Journal of Atmo-
 479 spheric and Terrestrial Physics*, *39*(9), 1041–1053. doi: 10.1016/0021-9169(77)
 480 90013-7
- 481 Maltsev, Yu. P., Leontyev, S. V., & Lyatsky, W. B. (1974). Pi-2 pulsations as a
 482 result of evolution of an Alfvén impulse originating in the ionosphere during
 483 a brightening of aurora. *Planetary and Space Science*, *22*, 1519–1533. doi:

- 484 10.1016/0032-0633(74)90017-8
 485 Menk, F. W., & Waters, C. L. (2013). *Magnetoseismology: Ground-based remote*
 486 *sensing of the earth's magnetosphere*. John Wiley and Sons. doi: 10.1002/
 487 9783527652051
- 488 Met Office. (2010 - 2015). Cartopy: a cartographic python library with a mat-
 489 plotlib interface [Computer software manual]. Exeter, Devon. Retrieved from
 490 <https://scitools.org.uk/cartopy>
- 491 Mikhailova, O. S., Smotrova, E. E., & Mager, P. N. (2022). Resonant generation
 492 of an alfvén wave by a substorm injected electron cloud: A van allen probe
 493 case study. *Geophysical Research Letters*, *49*(19), e2022GL100433. doi:
 494 10.1029/2022GL100433
- 495 Newton, R., Southwood, D., & Hughes, W. (1978). Damping of geomagnetic pulsa-
 496 tions by the ionosphere. *Planet. Space Sci.*, *26*, 201–209.
- 497 Obana, Y., Menk, F. W., Sciffer, M. D., & Waters, C. L. (2008). Quarter-wave
 498 modes of standing alfvén waves detected by cross-phase analysis. *Journal of*
 499 *Geophysical Research: Space Physics*, *113*(A8). doi: 10.1029/2007JA012917
- 500 Obana, Y., Waters, C. L., Sciffer, M. D., Menk, F. W., Lysak, R. L., Shiokawa, K.,
 501 ... Petersen, T. (2015). Resonance structure and mode transition of quarter-
 502 wave ulf pulsations around the dawn terminator. *Journal of Geophysical*
 503 *Research: Space Physics*, *120*(6), 4194–4212. doi: 10.1002/2015JA021096
- 504 Orr, D., & Matthew, J. A. D. (1971). The variation of geomagnetic micropulsation
 505 periods with latitude and the plasmopause. *Planetary and Space Science*, *19*,
 506 897–905. doi: 10.1016/0032-0633(71)90141-3
- 507 Ozeke, L. G., & Mann, I. R. (2004). Modeling the properties of guided poloidal
 508 alfvén waves with finite asymmetric ionospheric conductivities in a dipole
 509 field. *Journal of Geophysical Research: Space Physics*, *109*(A5). doi:
 510 <https://doi.org/10.1029/2003JA010151>
- 511 Petrashchuk, A. V., Klimushkin, D. Y., & Mager, P. N. (2022). Numeri-
 512 cal analysis of the spatial structure of Alfvén waves in a finite pressure
 513 plasma in a dipole magnetosphere. *Solar-Terrestrial Physics*, *8*, 3–12. doi:
 514 10.12737/stp-83202201
- 515 Pilipenko, V. A., Mazur, N. G., Fedorov, E. N., Engebretson, M. J., & Murr, D. L.
 516 (2005). Alfvén wave reflection in a curvilinear magnetic field and formation
 517 of Alfvénic resonators on open field lines. *Journal of Geophysical Research*,
 518 *110*(A9), 10. doi: 10.1029/2004JA010755
- 519 Radoski, H. R. (1967). Highly asymmetric MHD resonances. The guided
 520 poloidal mode. *Journal of Geophysical Research*, *72*, 4026–4033. doi:
 521 10.1029/JZ072i015p04026
- 522 Scholer, M. (1970). On the motion of artificial ion clouds in the magnetosphere.
 523 *Planet. Space Sci.*, *18*(7), 977–1004. doi: 10.1016/0032-0633(70)90101-7
- 524 Sciffer, M. D., & Waters, C. L. (2002). Propagation of ulf waves through the
 525 ionosphere: Analytic solutions for oblique magnetic fields. *Journal of Geo-*
 526 *physical Research: Space Physics*, *107*(A10), SIA 11-1-SIA 11-14. doi:
 527 10.1029/2001JA000184
- 528 Senior, A., Kosch, M. J., & Honary, F. (2008). Comparison of methods to
 529 determine auroral ionospheric conductances using ground-based opti-
 530 cal and riometer data. *Annales Geophysicae*, *26*(12), 3831–3840. doi:
 531 10.5194/angeo-26-3831-2008
- 532 Sinha, A., & Rajaram, R. (1997). An analytic approach to toroidal eigen mode.
 533 *Journal of Geophysical Research: Space Physics*, *102*(A8), 17649–17657.
- 534 Southwood, D. J. (1974). Some features of field line resonances in the magneto-
 535 sphere. *Planetary and Space Science*, *22*, 483–491. doi: 10.1016/0032-0633(74)
 536 90078-6
- 537 Southwood, D. J., & Hughes, W. J. (1983). Theory of hydromagnetic waves in
 538 the magnetosphere. *Space Science Reviews*, *35*(4), 301–366. doi: 10.1007/

- 539 BF00169231
540 Southwood, D. J., & Kivelson, M. G. (2001). Damping standing Alfvén waves in the
541 magnetosphere. *Journal of Geophysical Research Space Physics*, 106(6), 10829-
542 10836. doi: 10.1029/2000JA000343
- 543 Takahashi, K., & Denton, R. E. (2007). Magnetospheric seismology using multihar-
544 monic toroidal waves observed at geosynchronous orbit. *Journal of Geophysical*
545 *Research*, 112, A05204. doi: 10.1029/2006JA011709
- 546 Troitskaya, V. A., & Gul'elmi, A. V. (1967). Geomagnetic Micropulsations and
547 Diagnostics of the Magnetosphere. *Space Sci. Rev.*, 7(5-6), 689-768. doi: 10
548 .1007/BF00542894
- 549 Tsyganenko, N. A. (1996). Effects of the solar wind conditions in the global magne-
550 tospheric configurations as deduced from data-based field models. In (Vol. ESA
551 SP-389, p. 181-185).
- 552 Waters, C. L., Lysak, R. L., & Sciffer, M. D. (2013). On the coupling of fast and
553 shear Alfvén wave modes by the ionospheric Hall conductance. *Earth Planets*
554 *Space*, 65, 385-396. doi: 10.5047/eps.2012.08.002
- 555 Yoshikawa, A., & Itonaga, M. (1996). Reflection of shear Alfvén waves at the iono-
556 sphere and the divergent Hall current. *Geophysical Research Letters*, 23(1),
557 101-104. doi: 10.1029/95GL03580
- 558 Yoshikawa, A., Obana, Y., Shinohara, M., Itonaga, M., & Yumoto, K. (2002). Hall-
559 induced inductive shielding effect on geomagnetic pulsations. *Geophysical Re-*
560 *search Letters*, 29(8), 107-1-107-4. doi: 10.1029/2001GL013610